Advances in spectral electrical impedance tomography (sEIT) towards accurate imaging in the mHz to kHz frequency range

Haoran Wang[1], Johan Alexander Huisman[1], Egon Zimmermann[2], and Harry Vereecken[1]*
Correspondence: h .wang@fz-juelich.de
[1]Agrosphere (IBG 3), Institute of Bio- and Geosciences, Forschungszentrum Jülich GmbH, Jülich, Germany
[2]Electronic systems (ZEA-2), Central Institute of Engineering Electronics and Analytics, Forschungszentrum Jülich GmbH, Jülich, Germany

Summary

Spectral electrical impedance tomography (sEIT) has received an increased interest in recent years given its promising capability to image the subsurface complex electrical conductivity. However, there are a range of challenges that need to be addressed before sEIT will gain widespread acceptance. In this work, we present significant improvements in the sEIT method, including data inversion and electromagnetic (EM) coupling reduction. A novel complex inversion strategy was proposed and compared with existing strategies. It was found that the newly proposed complex inversion strategy can provide reliable inversion results especially in the presence of large phase angles. Data filtering methods were proposed to deal with EM coupling effects that affect the measurement accuracy above 50 Hz. With the use of the proposed data filters, we achieved plausible inversion results without correction for EM coupling effects up to 1 kHz.

Introduction

Spectral electrical impedance tomography (sEIT), also known as spectral complex resistivity tomography or spectral induced polarization tomography (SIP), is a non-invasive geophysical method that can image the complex electrical conductivity distribution of the subsurface in the frequency range from mHz to kHz. Laboratory studies have linked complex electrical conductivity measurements to material properties of interest, which accelerated the application of sEIT at the field scale in different contexts, including but not limited to hydrogeophysics and environmental engineering (Kemna et al., 2012).

To obtain reliable imaging results, a proper inversion strategy as well as accurate measurements are both important. The inversion of sEIT measurements is usually carried out for each frequency independently based on a two-step approach (Kemna, 2000; Martin and Günther, 2013; Johnson and Thomle, 2018). The two-step approach considers the separated treatment of the real and imaginary parts of the complex data and model in terms of data weighting and model regularization, but ignores the cross-sensitivity (i.e. the imaginary part of the complex sensitivity) assuming that the measured phase angles are small enough. This simplification needs further investigation given the fact that extremely large phase angles can be observed under certain circumstances (Kulenkampff and Yaramanci, 1993; Peruzzo et al., 2021). Moreover, to the best of our knowledge, there is no established method that can consider simultaneously the coupling between real and imaginary parts of the complex data and model, and the separated treatment in terms of data weighting and model regularization.

EM coupling effects including both inductive and capacitive coupling have long been an essential challenge in obtaining accurate sEIT measurements, especially at higher frequencies. Inductive coupling refers to the cable-to-cable effect. In particular, alternating current in an electrical wire creates a magnetic field, which induces a voltage in the wires for voltage measurements. Correction methods based on the mutual inductance to remove inductive coupling from sEIT measurements have been proposed and provided promising inversion results (Zimmermann et al., 2019). However, it is interesting to explore whether a careful selection of electrode configurations for sEIT measurements would allow to obtain reliable inversion results without the correction of inductive coupling. Capacitive coupling refers to the leakage of electric current through possible capacitances wherever a potential difference exists. Typically, three types of capacitive coupling are considered, between cables, between the ground and electrodes, and between the cable shield and the ground (or the materials of interest). With the use of coaxially shielded cables and distributed amplifiers for potential measurements, the first two types of capacitive coupling can be reduced to a large extent. To deal with the third type of capacitive coupling, Zimmermann et al. (2019) considered both integrated capacitances and leakage currents in the forward modelling during inversion of surface sEIT measurement. However, the corrections were only partly successful for higher frequencies. As in the case of inductive coupling, it is interesting to investigate whether reliable inversion results can be obtained by filtering out measurements that are strongly affected by capacitive coupling and to avoid corrections as much as possible.

The aim of this work is twofold. First, a novel complex inversion strategy will be proposed and compared with existing strategy. Second, two indices will be proposed to

quantify the inductive and capacitive coupling strength. The proposed indices will be used as data filters to select measurements for inversion without correction of EM coupling effects.

A novel complex inversion strategy

As in the inversion of DC resistivity data, EIT inversion relies on a Gauss-Newton approach to minimize the following objective function:

$$\Phi = \|\boldsymbol{W_d}(\boldsymbol{d} - f(\boldsymbol{m}))\|^2 + \lambda\|\boldsymbol{W}_m\boldsymbol{m}\|^2 \qquad (1)$$

where $\boldsymbol{d}$ is a vector with the measured data, $\boldsymbol{m}$ is a vector with model parameters, f ($\boldsymbol{m}$) is the forward response of model $\boldsymbol{m}$, $\boldsymbol{W}_d$ is a diagonal data weighting matrix, λ is the damping factor, and $\boldsymbol{W}_m$ is a regularization matrix used to specify the desired properties of the model $\boldsymbol{m}$. Here, the logarithmic of both the measured complex impedances and the complex electrical conductivity are considered as the complex form of data and model parameters. The two-step approach first inverts the amplitude of the measured complex impedances using a DC resistivity inversion routine. In the second step, the measured phase angles are inverted using the Jacobian matrix from the first step given the Cauchy-Riemann condition for the real part sensitivity.

Instead of directly using the complex form of data and model parameters, we extended the data vector to $\boldsymbol{d} = (\boldsymbol{ln}(|\boldsymbol{Z}^*|), \boldsymbol{\varphi_a})^T$ and the model parameter vector to $\boldsymbol{m} = (\boldsymbol{ln}(|\boldsymbol{\sigma}^*|), \boldsymbol{\varphi})^T$ in the improved complex inversion strategy. This results in an extended Jacobian matrix

$$\frac{\partial \boldsymbol{d}}{\partial \boldsymbol{m}} = \begin{pmatrix} \frac{\partial \boldsymbol{ln}(|\boldsymbol{Z}^*|)}{\partial \boldsymbol{ln}(|\boldsymbol{\sigma}^*|)} & \frac{\partial \boldsymbol{ln}(|\boldsymbol{Z}^*|)}{\partial \boldsymbol{\varphi}} \\ \frac{\partial \boldsymbol{\varphi_a}}{\partial \boldsymbol{ln}(|\boldsymbol{\sigma}^*|)} & \frac{\partial \boldsymbol{\varphi_a}}{\partial \boldsymbol{\varphi}} \end{pmatrix} \qquad (2)$$

which can be constructed using the complex sensitivity and the Cauchy-Riemann relations for both real and imaginary parts of sensitivity. An extended regularization matrix was defined that consists of two original regularization matrices at the main diagonal and two null matrices at the off-diagonal positions. To allow for different regularization strengths for the amplitude and phase, a diagonal damping matrix $\boldsymbol{L}$ instead of one single damping factor λ was used. Moreover, a 2D line-search procedure was proposed where the step lengths for the amplitude and phase were determined by fitting a six-point quadric surface.

A synthetic modelling experiment was carried out using the true model shown in Fig. 1 (a, b). There is an extremely large phase layer of 1000 mrad from -0.5 m to -2 m. The amplitude of the synthetic model was assumed to be homogeneous to demonstrate the effect of different inversion strategies. A dipole-dipole configuration using 21 electrodes with 1 m electrode spacing was adopted to simulate the measured complex impedances. The modelled complex impedances were contaminated with 3% relative error for the amplitude of impedance and a 5 mrad absolute error for the phase, which were also used for the error-weighted inversion.

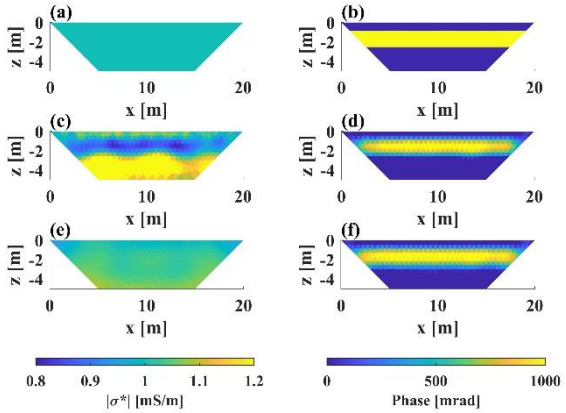

Figure 1: Amplitude and phase angle of complex electrical conductivity for the True model (a, b), inverted model using two-step strategy (c, d), and inverted model using improved complex inversion strategy (e, f).

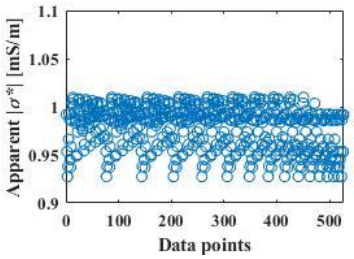

Figure 2: The amplitude of modelled apparent electrical conductivity using the true model presented in Fig.1(a and b)

The inversion results presented in Fig.1 clearly showed that the two-step inversion failed to resolve the amplitude of the electrical conductivity, while the improved complex inversion presented plausible results. The reason for the failure of two-step strategy can be explained by the modelled amplitude of the apparent conductivity shown in Fig.2. In the case of ERT or EIT data with small phases, the modelled apparent electrical conductivity for a homogeneous model of 1 mS/m should be expected to be 1 mS/m. Due to the extremely large phase angles, the modelled apparent electrical conductivity ranges from 0.9 to 1.02, which results in differences from 2% to 10%. Therefore, DC resistivity inversion without considering the complex coupling is not suitable in the case of large phase angles.

EM coupling removal in field sEIT measurements

A custom-made 40-channel sEIT measurement system (Zimmermann et al., 2008) was used to obtain the field sEIT measurements. The system measures the voltage relative to the system ground at all electrodes except the two current electrodes. The potential difference for a four-pole electrode configuration can then be calculated in a post-processing step. For each excitation, the system measures the excitation currents through both the positive and negative current poles. With this additional information, the leakage current can be calculated and the total capacitance between the cable shield and ground can be derived. The field measurements used in this study have previously been presented by Zimmermann et al. (2019) and used the fan-shaped cable layout shown in Fig.3. Measurements were acquired at two locations near Milano, Italy with different electrical properties of the subsurface. Site A is located near Senna Lodigiana in the Lodi plain along a terrace of the Po river. This site showed a low bulk electrical conductivity. Site B is located near Lozzolo and the soil has a high electrical conductivity. Zimmermann et al. (2019) already showed that inductive coupling was negligible at site A and that the capacitive coupling dominated the measurement accuracy at site B.

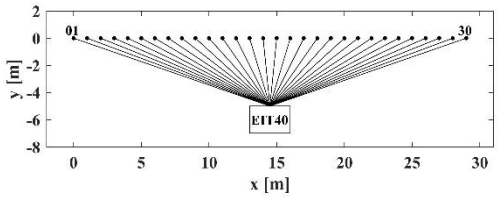

Figure 3: The fan-shaped cable layout used for field measurements

To deal with the inductive coupling, we propose an index to evaluate the inductive coupling strength (ICS) for a certain configuration. The ICS is defined as the ratio of the frequency dependent mutual inductance ωM and the imaginary part impedance Z_0'' induced by the soil polarization. Z_0'' was calculated using a homogenous model of 10 mS/m and a phase angle of 30 mrad based on the inversion results of Zimmermann et al. (2019).

$$ICS = 100 \times \left| \frac{\omega M}{Z_0''} \right| \ (\%) \qquad (3)$$

ICS values were calculated using the highest measurements frequency that was considered, and a threshold ICS value of 5% was applied to select configurations that are unlikely to be strongly affected by inductive coupling. Fig.4 compares the inversion results obtained by a complete dataset and the ICS-filtered dataset for three selected frequencies. Without correction for inductive coupling, the results of the complete dataset showed inconsistent imaging results at the highest frequency and a high relative RMS error. The inversion results obtained with the ICS-filtered configurations showed good spectral consistency and a reasonable relative RMS error even at the highest frequency. For a more detailed investigation about the removal of inductive coupling by filtering, we refer to Wang et al. (2021).

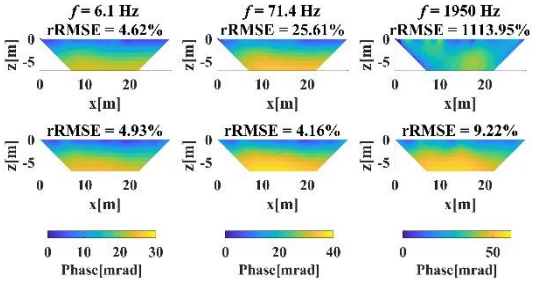

Figure 4: Inverted phase distribution for site B using the complete datasets (top row) and the ICS-filtered datasets (bottom row).

Capacitive coupling strongly depends on the distribution of the real part of the electrical conductivity and the resulting potential distribution, which are heterogeneous and unknown a priori. By assuming that only capacitive coupling needs to be considered and that other sources of measurement error are of secondary importance, an index was proposed to quantify the capacitive coupling strength (CCS) of each configuration. CCS is defined as the ratio of the imaginary part impedance Z_c'' induced by the capacitive coupling and the imaginary part impedance due to the soil polarization, which can be calculated by extracting Z_c'' from the measured imaginary part impedance Z_m'':

$$CCS = 100 \times \left| \frac{Z_c''}{Z_m'' - Z_c''} \right| \ (\%) \qquad (4)$$

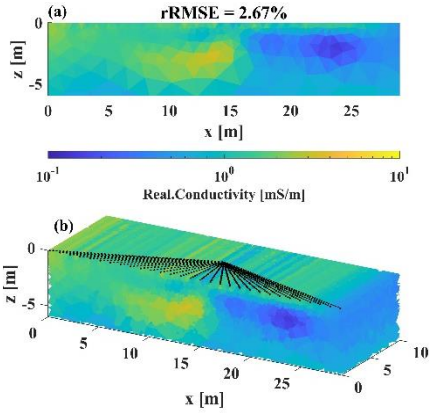

Figure 5: (a) 2D inversion result for the real part of the electrical conductivity; (b) 3D conductivity model with integrated capacitances (black dots).

Following the modelling strategy of Zimmermann et al. (2019), we found that Z_c'' can be calculated when

information is available for the real part of the electrical conductivity distribution, the total capacitance, and the leakage currents. Therefore, we propose the following procedure to calculate CCS. In the first step, the real part of the impedances are inverted to obtain the 2D electrical conductivity distribution. In a second step, the 2D distribution is mapped to a 3D model and the total capacitance is distributed homogeneously along the cable layout in the 3D model as shown in Fig.5. In a third step, the 3D FEM modelling with integrated capacitances and leakage current is performed to obtain Zc''. In the final step, the CCS values of all measurements are calculated using Eq. (4).

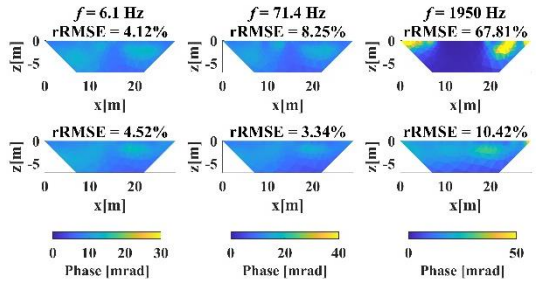

Figure 6: Inverted phase distribution for site A using the complete datasets (top row) and the CCS-filtered datasets (bottom row).

After the calculation of CCS, we selected measurements with CCS values below 5% for the highest frequency. Fig. 6 shows the inversion results obtained by a complete dataset and the CCS-filtered dataset. The inverted phase angle at the highest frequency produced by the complete configuration presented extremely low phase values, which is not in agreement with results at lower frequencies. The results produced by the CCS-filtered configurations showed good spectral consistency and the relative RMS errors were much lower.

Conclusions and outlook

In this study, we presented advances in the sEIT method towards accurate imaging of the complex electrical conductivity distribution. First, a novel complex inversion strategy that can simultaneously consider the coupling between real and imaginary parts of the complex data and model, and the separated treatment of the real and imaginary part in terms of data weighting and model regularization was proposed. The newly proposed inversion strategy was compared with a two-step inversion approach. It was found that the improved complex inversion strategy can produce reasonable inversion results even in the case of extremely large phase angles. In addition, data filtering methods were proposed to deal with EM coupling effects. With the use of the proposed data filters, we achieved plausible inversion results without correction for EM coupling effects up to the kHz frequency range. The proposed data filter for inductive coupling can be directly applied to any other measurement system. However, the method for capacitive coupling is currently limited to customized data acquisition systems. In future studies, the following three steps could be considered to further reduce capacitive coupling: (1) apply the proposed method with a centralized multiplexer and a fan-shaped cable layout; (2) use shielded multicore cable bundles; (3) develop strategies to measure leakage currents for commercially available measurement systems.

References

Johnson, T. C., and Thomle, J. (2018). 3-d decoupled inversion of complex conductivity data in the real number domain. *Geophysical Journal International, 212*(1), 284-296.

Kemna, A. (2000). Tomographic inversion of complex resistivity. *Ruhr-Universität Bochum*.

Kemna, A., Binley, A., Cassiani, G., Niederleithinger, E., Revil, A., Slater, L., et al. (2012). An overview of the spectral induced polarization method for near-surface applications. *Near Surface Geophysics, 10*(6), 453-468.

Kulenkampff, J. M., and Yaramanci, U. (1993). Frequency-dependent complex resistivity of rock-salt samples and related petrophysical parameters. *Geophysical Prospecting, 41*(8), 995-1008.

Martin, T., and Günther, T. (2013). Complex resistivity tomography (crt) for fungus detection on standing oak trees. *European Journal of Forest Research, 132*(5-6), 765-776.

Peruzzo, L., Liu, X., Chou, C., Blancaflor, E. B., Zhao, H., Ma, X. F., et al. (2021). Three‐channel electrical impedance spectroscopy for field‐scale root phenotyping. *The Plant Phenome Journal, 4*(1), e20021.

Wang, H., Huisman, J. A., Zimmermann, E., and Vereecken, H. (2021). Experimental design to reduce inductive coupling in spectral electrical impedance tomography (seit) measurements. *Geophysical Journal International, 225*(1), 222-235.

Zimmermann, E., Huisman, J. A., Mester, A., and van Waasen, S. (2019). Correction of phase errors due to leakage currents in wideband eit field measurements on soil and sediments. *Measurement Science and Technology, 30*(8).

Zimmermann, E., Kemna, A., Berwix, J., Glaas, W., and Vereecken, H. (2008). Eit measurement system with high phase accuracy for the imaging of spectral induced polarization properties of soils and sediments. *Measurement Science and Technology, 19*(9).